Supplementary Information

Plasma-Mediated Fabrication of Ultrathin NiAl Nanosheets Having Rich Oxygen Vacancies and Doped Nitrogen Sites and Their Utilization for High Activity and Robust Stability in Photoelectrochemical Water Oxidation

Keon-Han Kim[a], Jae Won Choi[b], Heebin Lee[b], Byeong Cheul Moon[b], Dong Gyu Park [b], Won Ho Choi [b] and Jeung Ku Kang[a,b,*]*

[a]Department of Materials Science and Engineering, Korea Advanced Institute of Science and Technology (KAIST), 291 Daehak-ro, Yuseong-gu, Daejeon 34141, Republic of Korea

[b]Graduate School of Energy, Environmental, Water and Sustainability (EEWS), Korea Advanced Institute of Science and Technology (KAIST), 291 Daehak-ro, Yuseong-gu, Daejeon 34141, Republic of Korea

*Corresponding authors: jeungku@kaist.ac.kr

Table of Contents

Section S1. Experimental Details

Chemicals: All chemicals used in the synthesis of materials were purchased from Sigma Aldrich. Also, ethanol and distilled water were purchased from Duksan. In addition, all chemicals were used as received in air.

Synthesis of layered double hydroxide nanoplates: NiAl layered double hydroxide nanoplates were synthesized in two steps using co-precipitation and hydrothermal methods. At first, an aqueous solution of sodium carbonate (1.0 M) and sodium hydroxide (1.0 M) was pre-heated in a one-neck flask at 60℃. The metal precursor aqueous solution (0.64 M) was added to a pre-heated solution in a drop-wise manner. The metal precursor solution was prepared by dissolving 0.48 M nickel nitrate hexahydrate and 0.16 M aluminum nitrate nonahydrate in DI water. The reaction was proceeded for 24 h with refluxing. After co-precipitation, the solution was crystalized in the Teflon-made vessel with a stainless steel autoclave for 24 h at 110 ℃. The produced solution was centrifuged several times at 6000 rpm for 10 min with water and ethanol. Finally, the centrifuged powder was dried at 50℃ in a vacuum oven overnight.

Fabrication of chemically exfoliated layered double hydroxide nanosheets: NiAl layered double hydroxide nanoplates were synthesized in two steps using co-precipitation and hydrothermal methods. At first, an aqueous solution of sodium nitrate (1.0 M) and sodium hydroxide (1.0 M) was pre-heated in a one-neck flask at 60℃. Then, the metal precursor aqueous solution (0.64 M), which was prepared by dissolving 0.48 M nickel nitrate hexahydrate and 0.16 M aluminum nitrate nonahydrate in DI water, was added to the pre-heated solution in a drop-wise manner. Next, the reaction was proceeded for 24 h with refluxing. After co-precipitation, the solution was crystalized in the Teflon-made vessel with a stainless steel autoclave for 24 h at 110 ℃. Then, the produced solution was centrifuged several times at 6000 rpm for 10 min with water and ethanol. Finally, the centrifuged powder was dried at 50℃ in a vacuum oven overnight. The 1 g of dried powder was mixed with 1L of formamide and stirring for 24 hours. After finishing stirring, the solution was sonicated for 2 days to exfoliate. After stirring and sonication, the produced solution was filtered with water and ethanol several times and dried at 50℃ in a vacuum oven overnight.

Fabrication of N-doped NiAl nanosheets: The N-doped NiAl nanosheets were synthesized by nitrogen plasma treatment during several minutes. The as-prepared NiAl LDH nanoplates were put inside the microwave plasma enhanced-chemical vapor deposition (MPE-CVD) equipment. (Richardson Electronics microwave generator) Plasma ball was created center on the chamber of MPE-CVD through 500 W microwave power with N_2 (99.999%) gas flow of 100 sccm at room temperature. By changing the plasma treatment time to 3, 7 and 15 min, N3, N7 and N-doped NiAl nanosheets could be fabricated, respectively.

Synthesis of hematite: Hematite was synthesized via two step annealing process with substrate of the F-doped SnO_2 coated glass substrate (FTO glass, 1 cm x 2 cm). FTO glass was ultrasonically washed with water, acetone and ethanol for 10 min, respectively. The synthesis proceeded in the Teflon-made vessel with a stainless steel autoclave with 0.15 M $FeCl_3$ and 1 M $NaNO_3$ aqueous solution (pH = 1.5, pH was controlled by adding HCl). The convection oven (Heratherm OMS60, Thermoscientific) was set at 100 °C, and the autoclave was put into the convection oven for 135 min. As-prepared yellowish thin film was gently rinsed with deionized (DI) water, and then annealed at 550 °C for 1 h and 750 °C for 20 min, in order.

Fabrication of photoanodes: At first, all of co-catalyst samples were dispersed in DI water with the concentration of 2 g/L. Then, 50 μL of solution was spread on Hematite photoanode and spin coated with 2000 rpm during 30 s. It is notable that the numbers for spin coating could achieve the different contents of co-catalysts. At the end of spin coating, the fabricated photoanodes were annealed at 80 °C for 1 hour.

Characterizations: The powder X-ray diffraction (PXRD) patterns were measured with a Smartlab diffractometer (Rigaku, Japan) using a Cu kα operating condition of 40 kV and 30 mA, where the diffraction patterns were scanned from 3° to 70° with a 0.02 step size. The Fourier transform-infrared (FT-IR) spectra were collected with the ATR using FT-TR-6100 from JASCO with a range of 1000 cm^{-1} ~ 4000 cm^{-1}, Moreover, Scanning electron microscopy images were gained using a JSM-7600F, JEOL and transmission electron microscopy (TEM) and high resolution-transmission electron microscopy (HR-TEM) images were obtained with a JEM-ARM200F model (JEOL Ldt., Japan). Additionally, the x-ray absorption near edge structure (XANES) and Extended X-ray Absorption Fine Structure (EXAFS) measurements were conducted in a 7D beam line at the Pohang Accelerating Laboratory (PAL, Republic of Korea), where a calibration of each K-edge spectrum was accomplished by employing the reference spectrum from the corresponding metal foil while the calibration was performed using the reference spectrum of W foil in the case of Ga. The XPS spectra were gained by using the K-alpha instrument (Thermo Scientific) equipped with the Al Ka micro-focused X-ray

monochromator (1487 eV). Raman spectra were also obtained by a dispersive Raman spectrometer (Horiba Jobin Yvon, ARAMIS) with 514 nm of Ar ion CW laser. Evolved oxygen and hydrogen gases were detected by a GC 7890A column (Agilent Technologies, United States) equipped with 5 Å molecular sieves with a thermal conductivity detector.

IPCE measurement: The 150 W Xe arc lamp (ABET) with a monochromator (Dongwoo Optron MonoRa-500i) was utilized as the light source in the dark box and The Peccell PEC-SI02 Si photodiode was used for a calibration of the IPCE value based on the following equation of

$$\text{IPCE (\%)} = (J_{photo} \times 1239.8) \,/\, (P_{int} \times \lambda_{int}) \times 100\ (\%)$$

where J_{photo} is the photocurrent density from a sample at a specific wavelength, P_{int} is the power intensity of incident light at a specific wavelength, and λ_{int} is the wavelength of incident light.

Photoelectrochemical water oxidation catalyst test: All the photoelectrochemical measurements were carried out by using PINE Instrument Quartz Photoelectrochemical Cell kit to the potentiostat (Biologic SP-240). The Pt counter electrode and Hg/HgO reference electrode were used to measure photoelectrochemical water oxidation properties. An aqueous electrolyte of 1 M KOH (pH 14) was continuously purged with He gas (99.999%) during reaction. 300 W Xe arc lamp (ORIEL) attached with NEWPORT liquid (infra-red light) filter, light shaping diffuser (homogenizer), and AM 1.5G filter were used for a light irradiation and intensity of light is one sun condition (100 mW/cm^2). The scan rate of the photocurrent-voltage curve was 10 mV/s. The measured potentials (vs. the Hg/HgO) were converted into the reversible hydrogen electrode (V_{RHE}) scale by using the Nernst equation

$$V_{RHE} = V_{Hg/HgO} + 0.059 \times pH + V^{o}_{Hg/HgO\ vs.\ NHE}$$

,where $V_{Hg/HgO}$ is the experimental penitential value against the 1M KOH Hg/HgO reference electrode, pH is 14 at a 1 M KOH aqueous solution and $V^{o}_{Hg/HgO\ vs.\ NHE}$ is 0.098 V at 25 °C.

Section S2. Supporting Figures

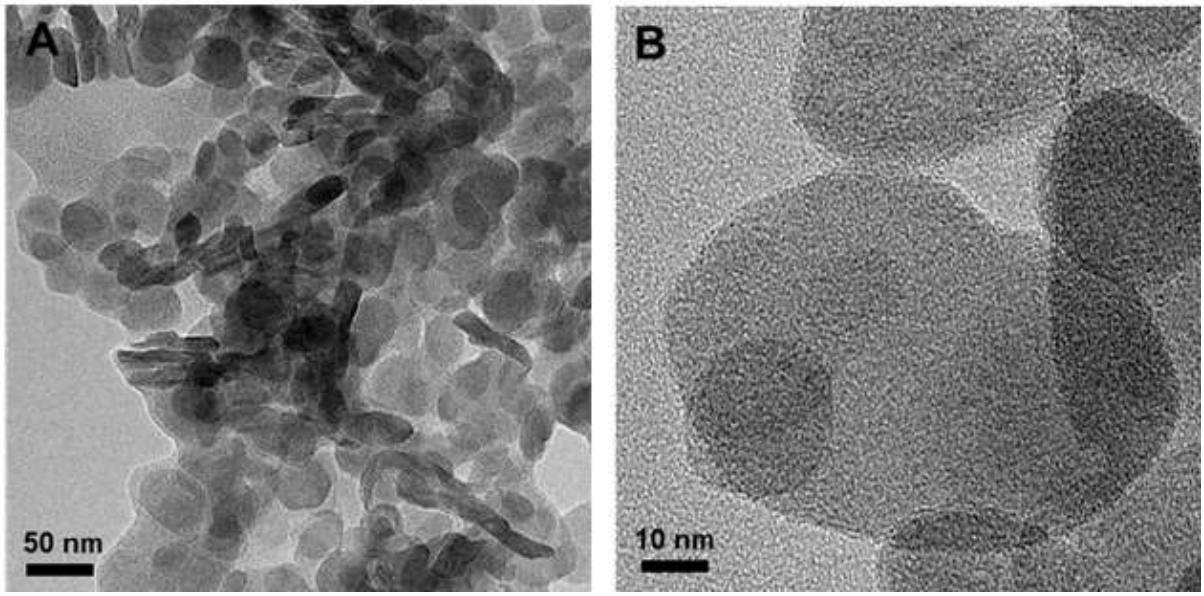

Figure S1. (A) TEM images of NiAl LDH and (B) a high magnification image of NiAl LDH nanoplates.

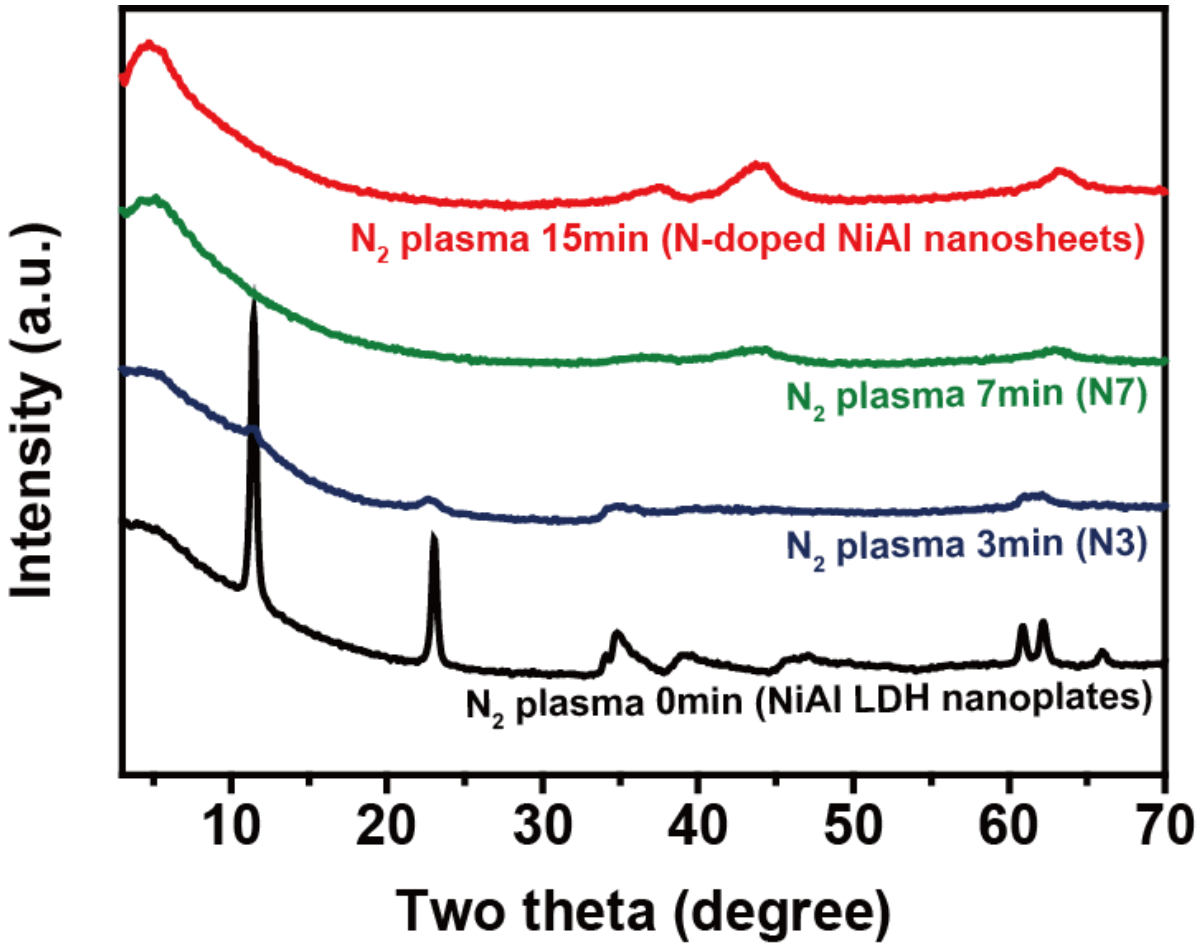

Figure S2. PXRD patterns of NiAl LDH nanoplates, N3, N7 and N-doped NiAl nanosheets.

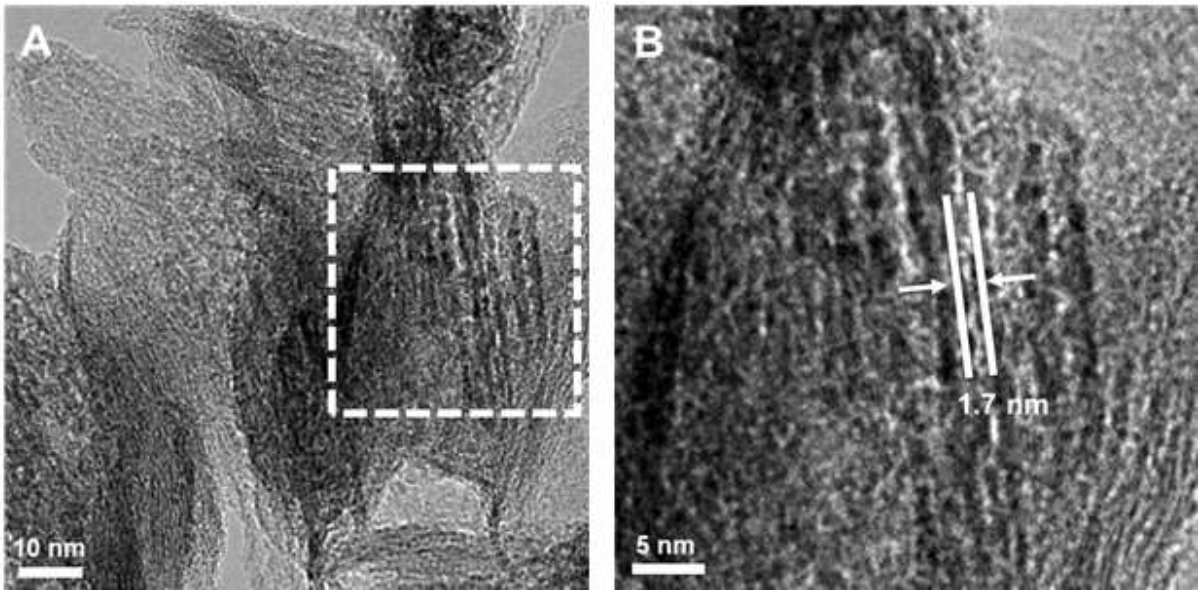

Figure S3. (A) TEM images of N-doped NiAl nanosheets which were exfoliated region matched well with a 5 ° peak using Bragg's law in Figure 2A and (B) its magnified region.

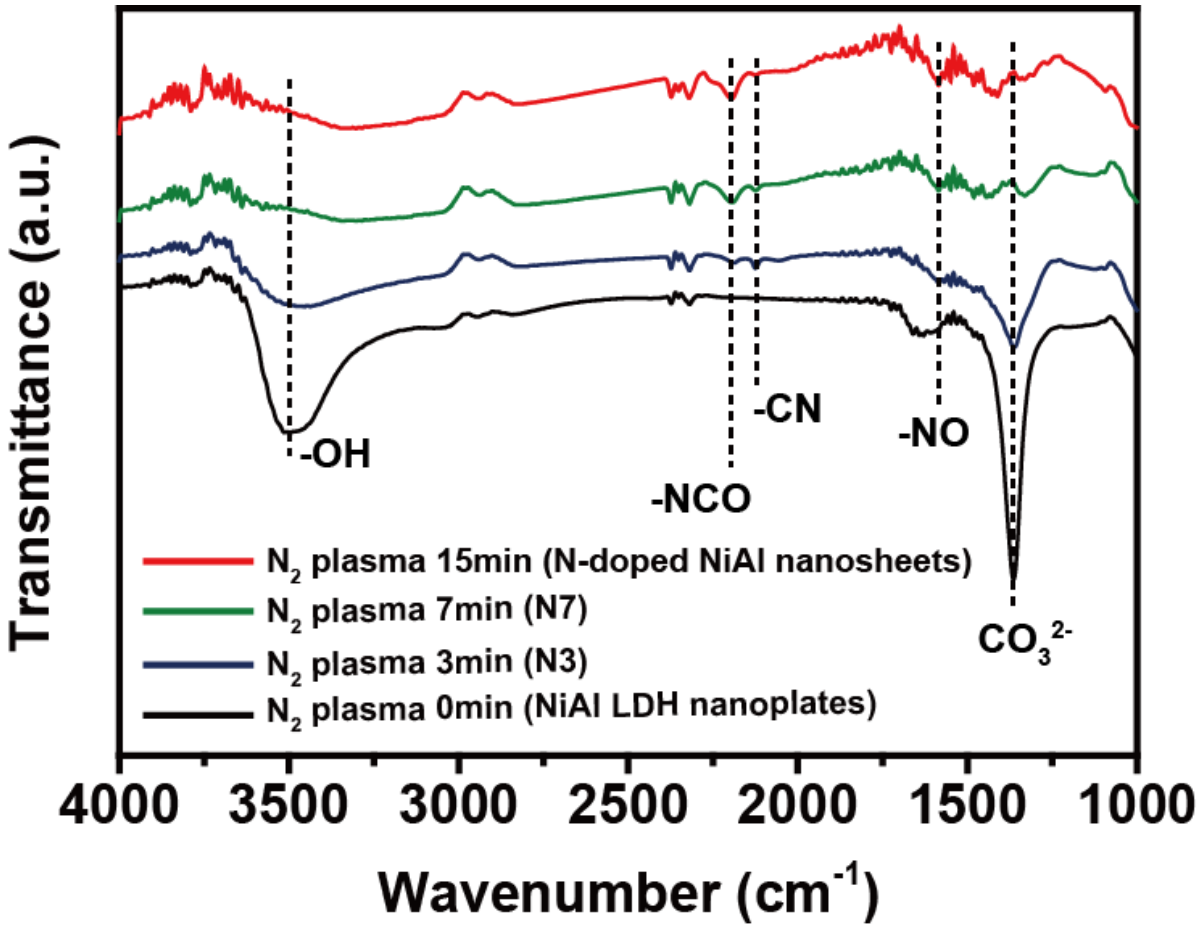

Figure S4. FT-IR spectra of NiAl LDH nanoplates, N3, N7 and N-doped NiAl nanosheets.

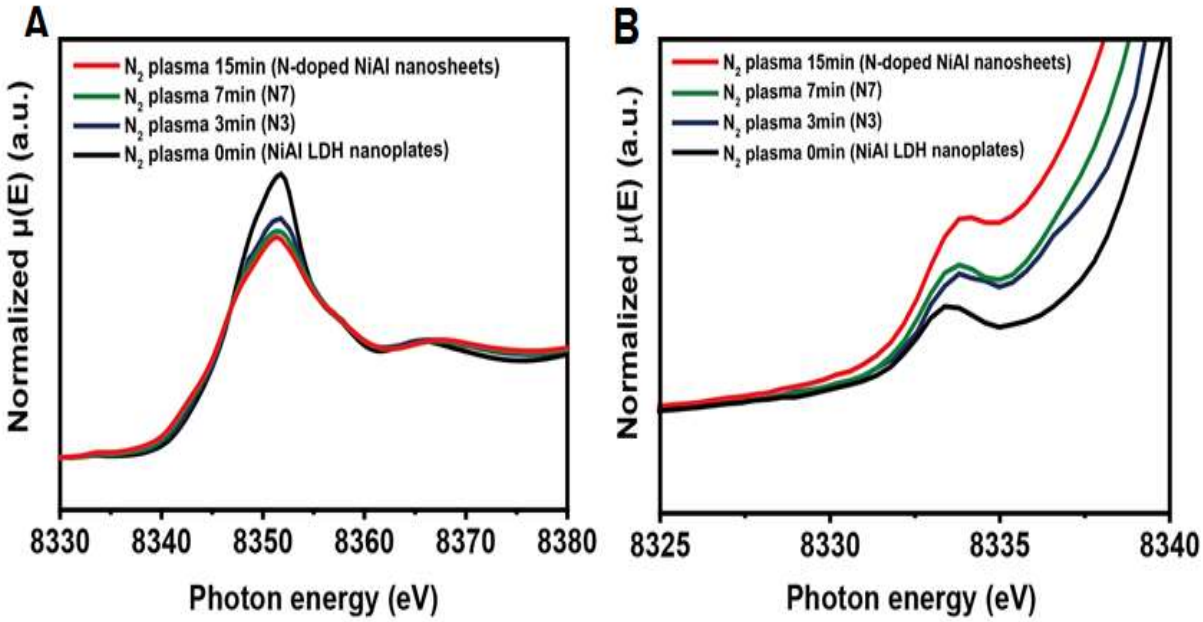

Figure S5. (A) Ni K-edge XANES spectra magnified around 8333 eV of NiAl LDH nanoplates, N3, N7 and N-doped NiAl nanosheets and (B) pre-edge region enlarged around 8333 eV.

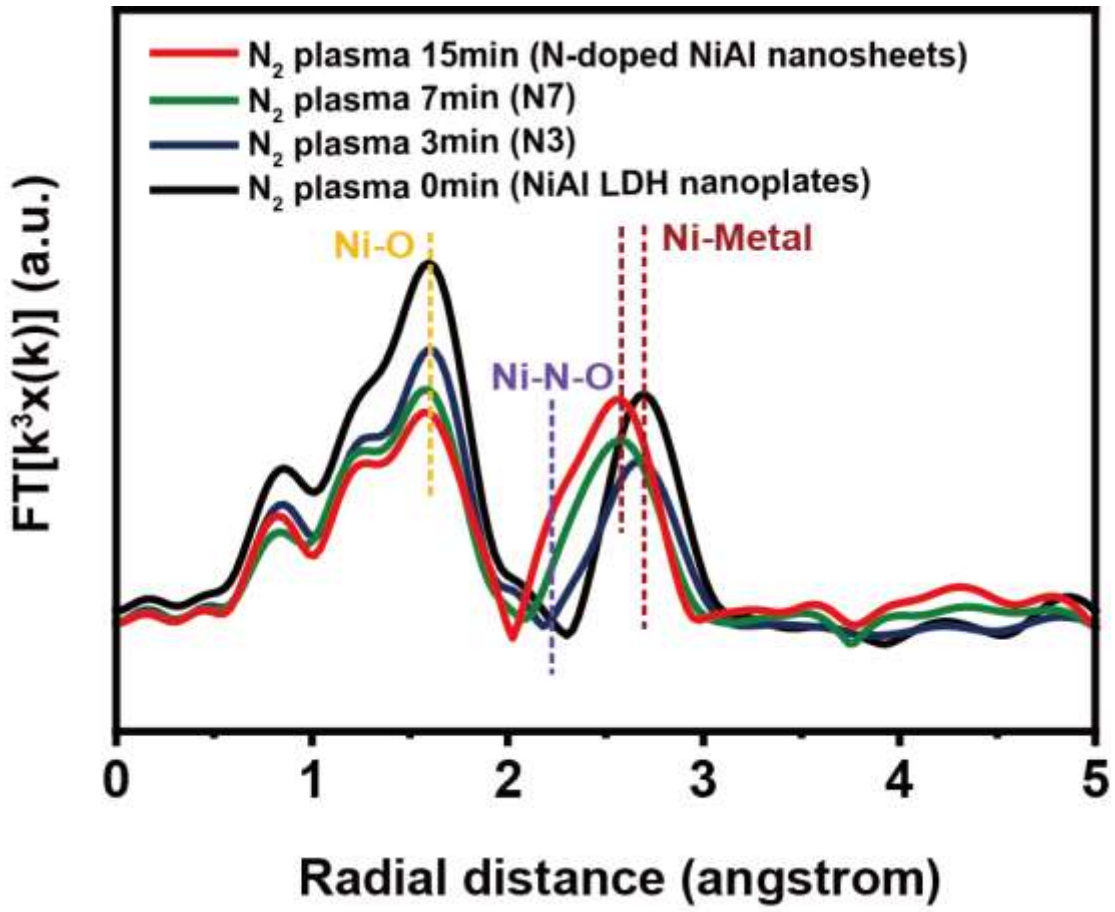

Figure S6. Fourier transformed EXAFS data of NiAl LDH nanoplates, N3, N7 and N-doped NiAl nanosheets.

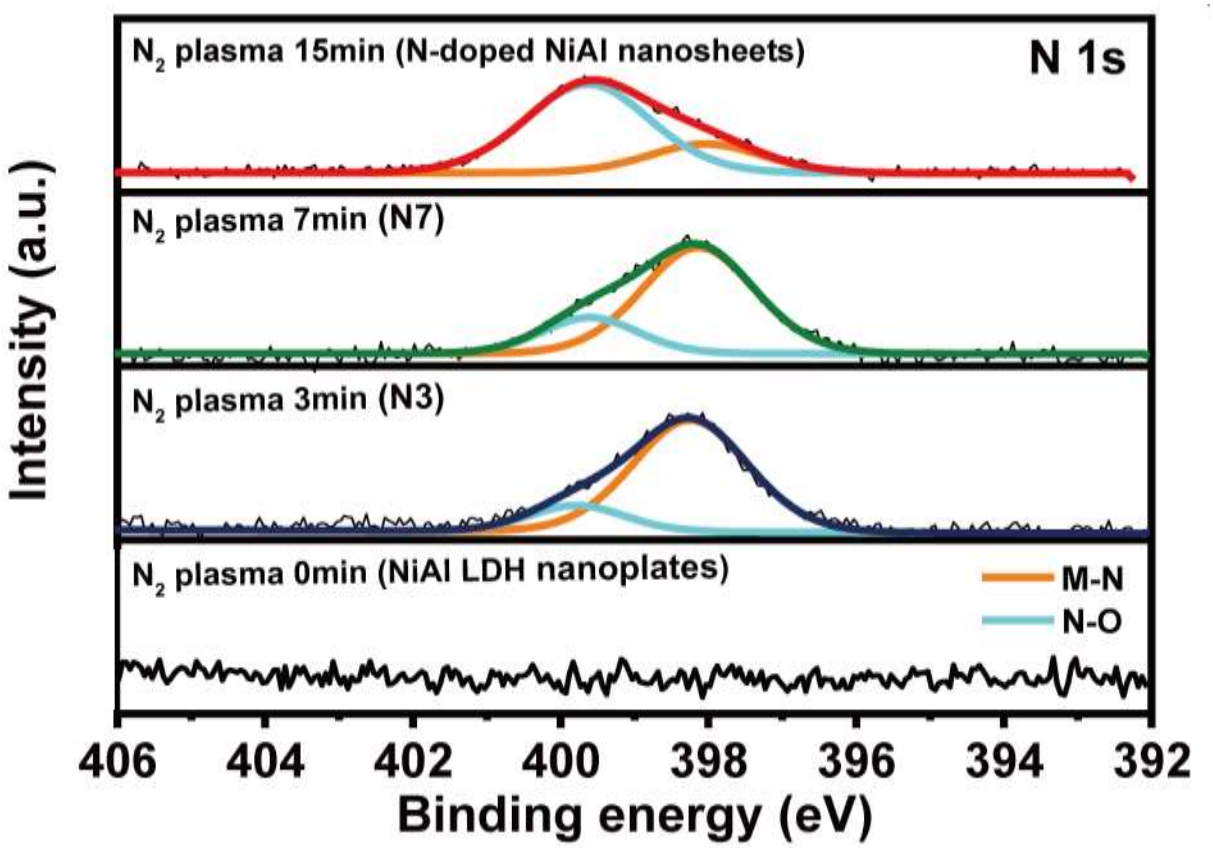

Figure S7. XPS spectra for N 1s orbitals of NiAl LDH nanoplates, N3, N7 and N-doped NiAl nanosheets.

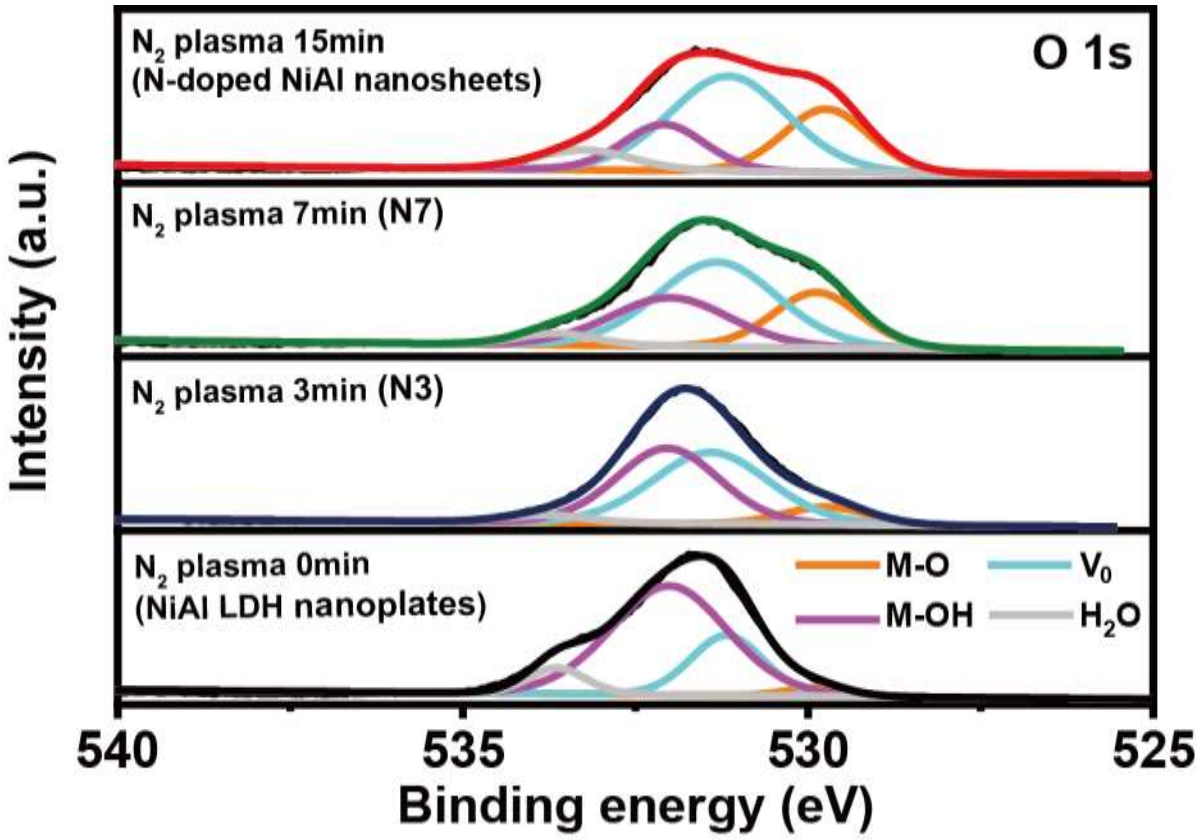

Figure S8. XPS spectra for O 1*s* orbitals of NiAl LDH nanoplates, N3, N7 and N-doped NiAl nanosheets.

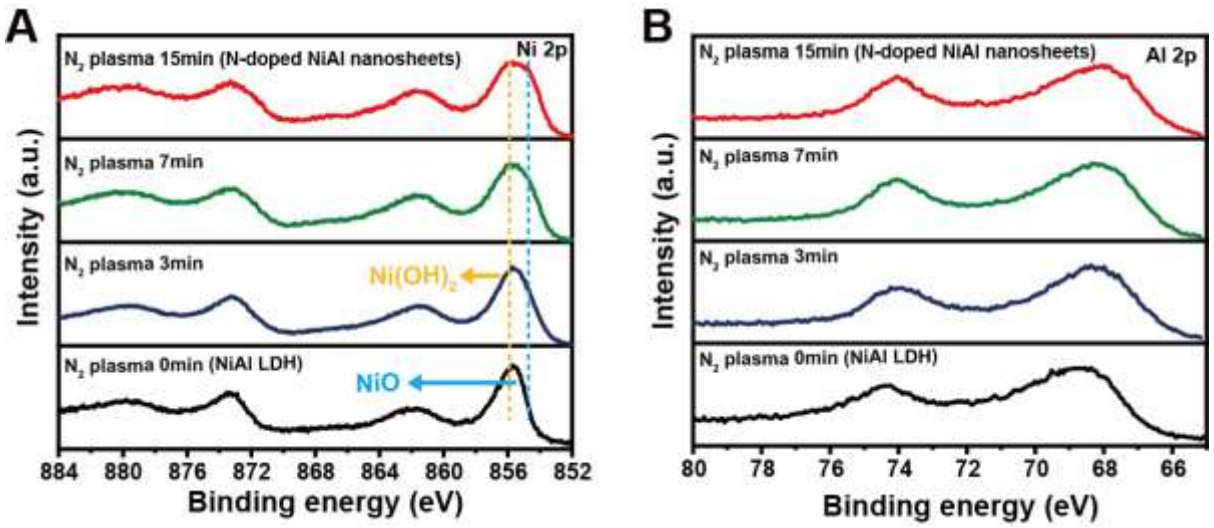

Figure S9. XPS spectra for (A) Ni 2p and (B) Al 2p orbitals of NiAl LDH nanoplates, N3, N7 and N-doped NiAl nanosheets.

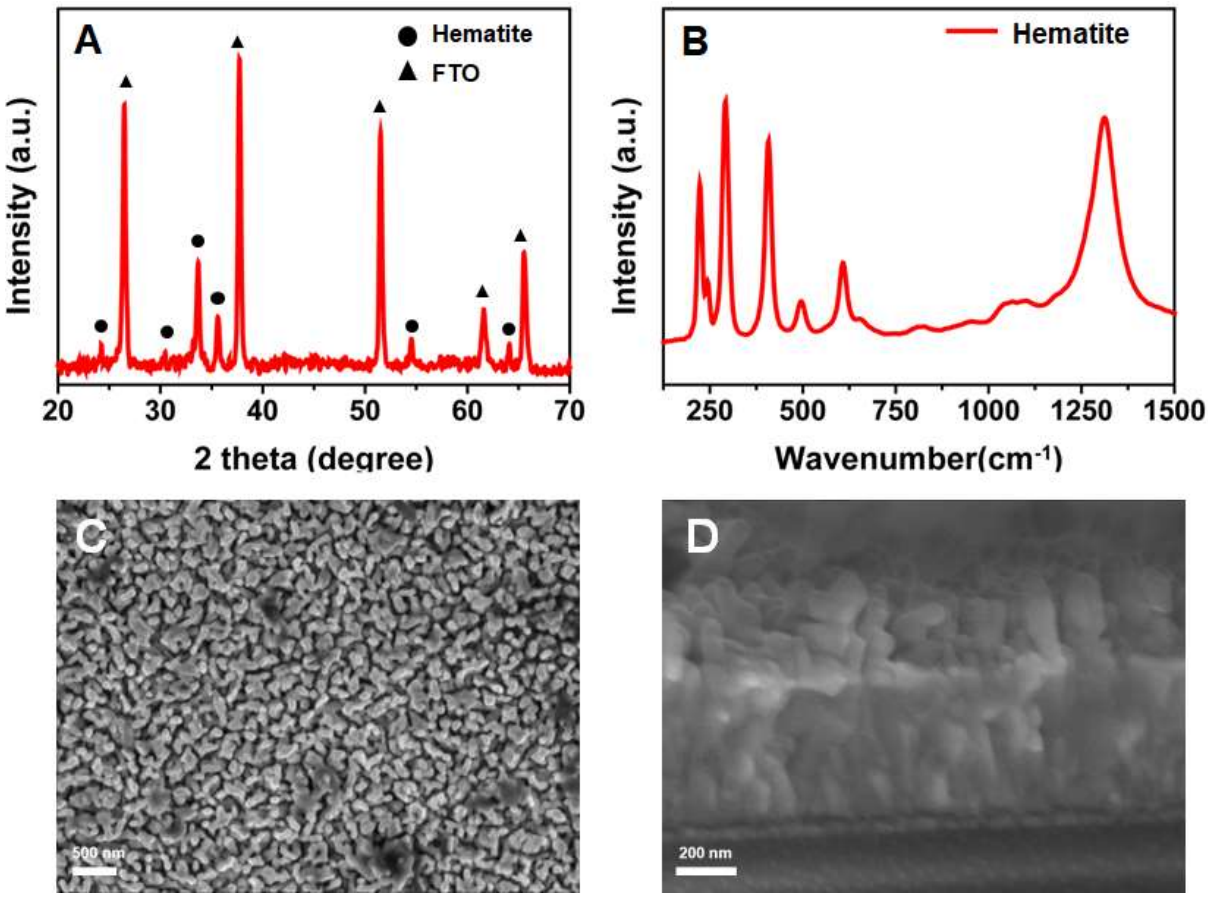

Figure S10. (A) PXRD patterns of α-Fe_2O_3/FTO. (B) Raman spectrum of α-Fe_2O_3. SEM (C) image and (D) cross-section image of α-Fe_2O_3.

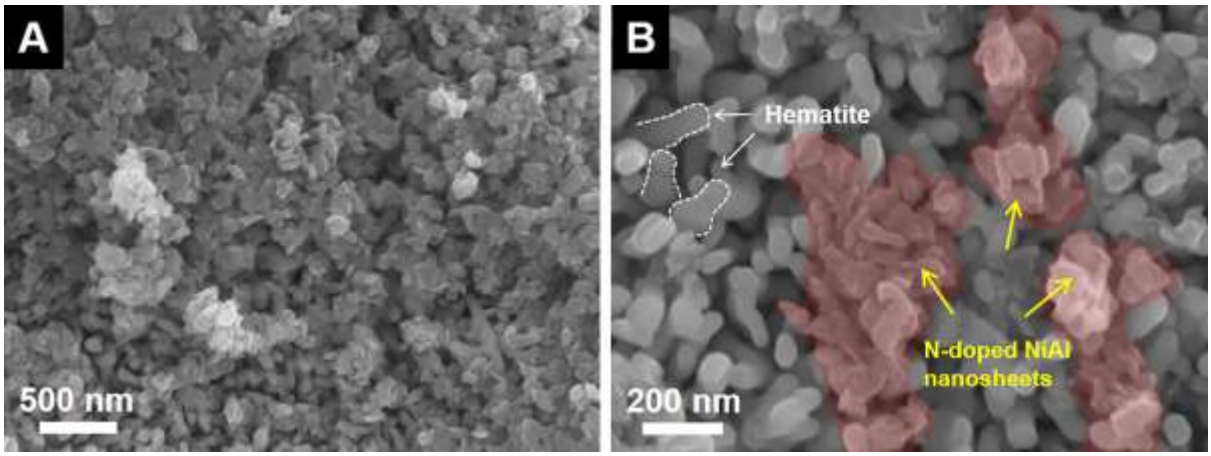

Figure S11. The SEM images of N-doped NiAl nanosheets on Hematite nanorods (A) at low and (B) high magnification.

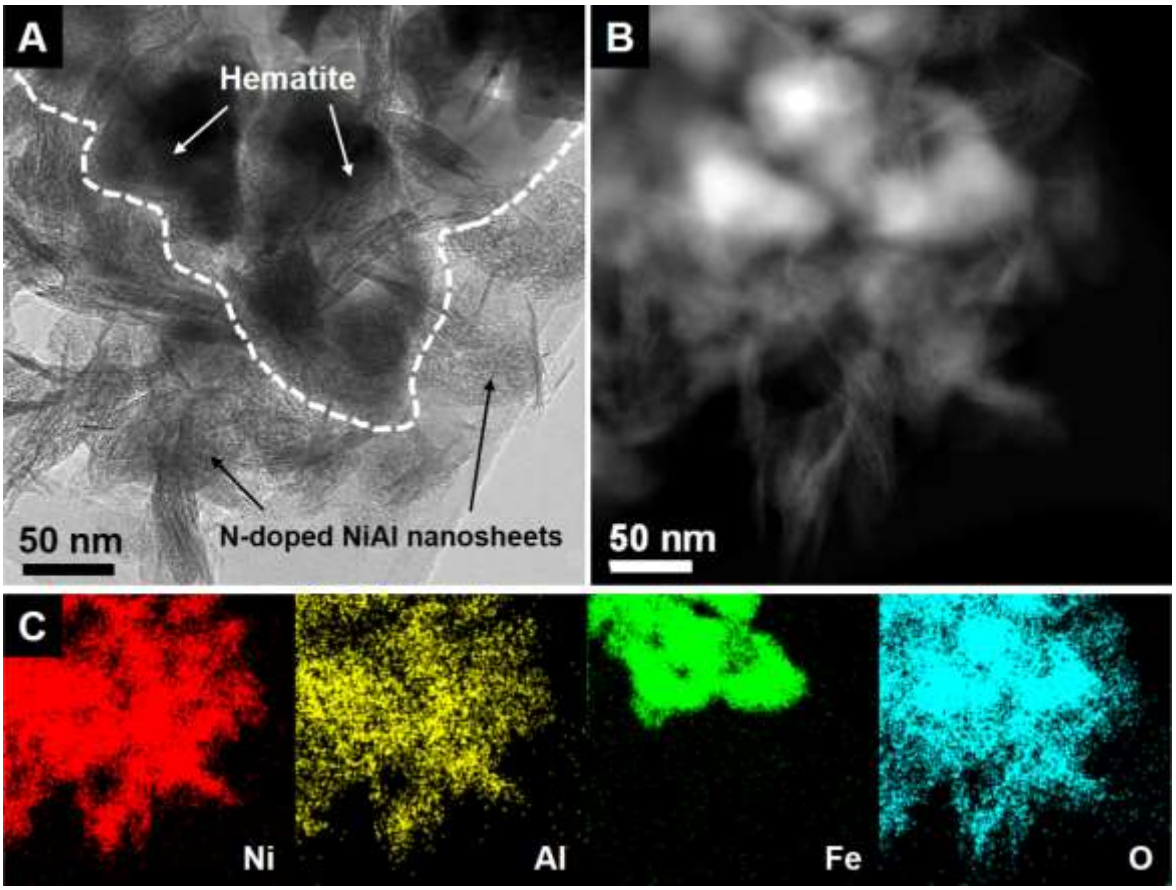

Figure S12. (A) The HRTEM image, (B) STEM HADDF image, and (C) EDS mapping images of N-doped NiAl nanosheets assembled on Hematite.

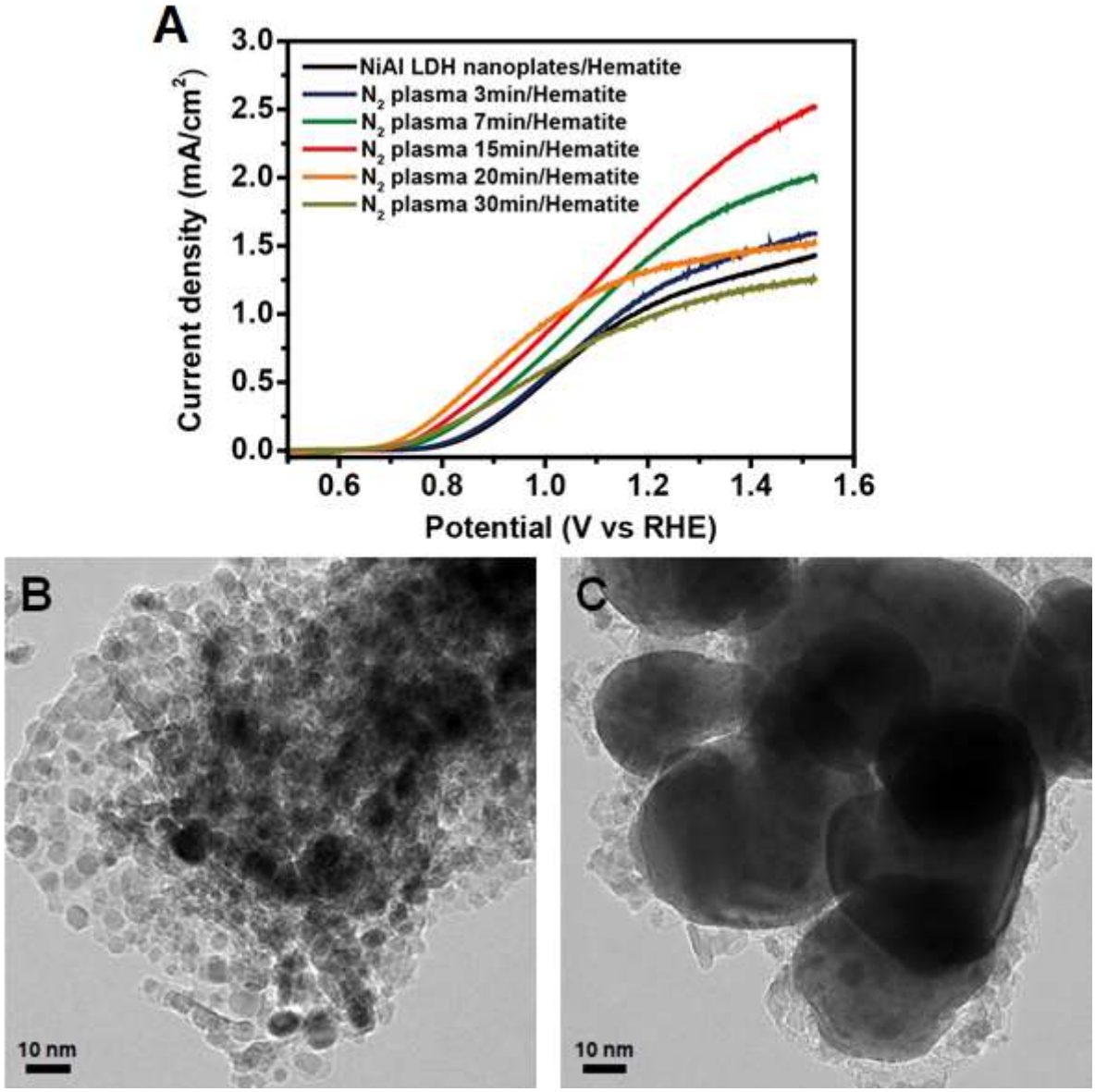

Figure S13. (A) The curves for photocurrent versus potential on NiAl LDH nanoplates as well as N-doped NiAl nanosheets corresponding to N3, N7, N15, N20 and N30 samples. TEM image of (B) N20 and (C) N30 samples.

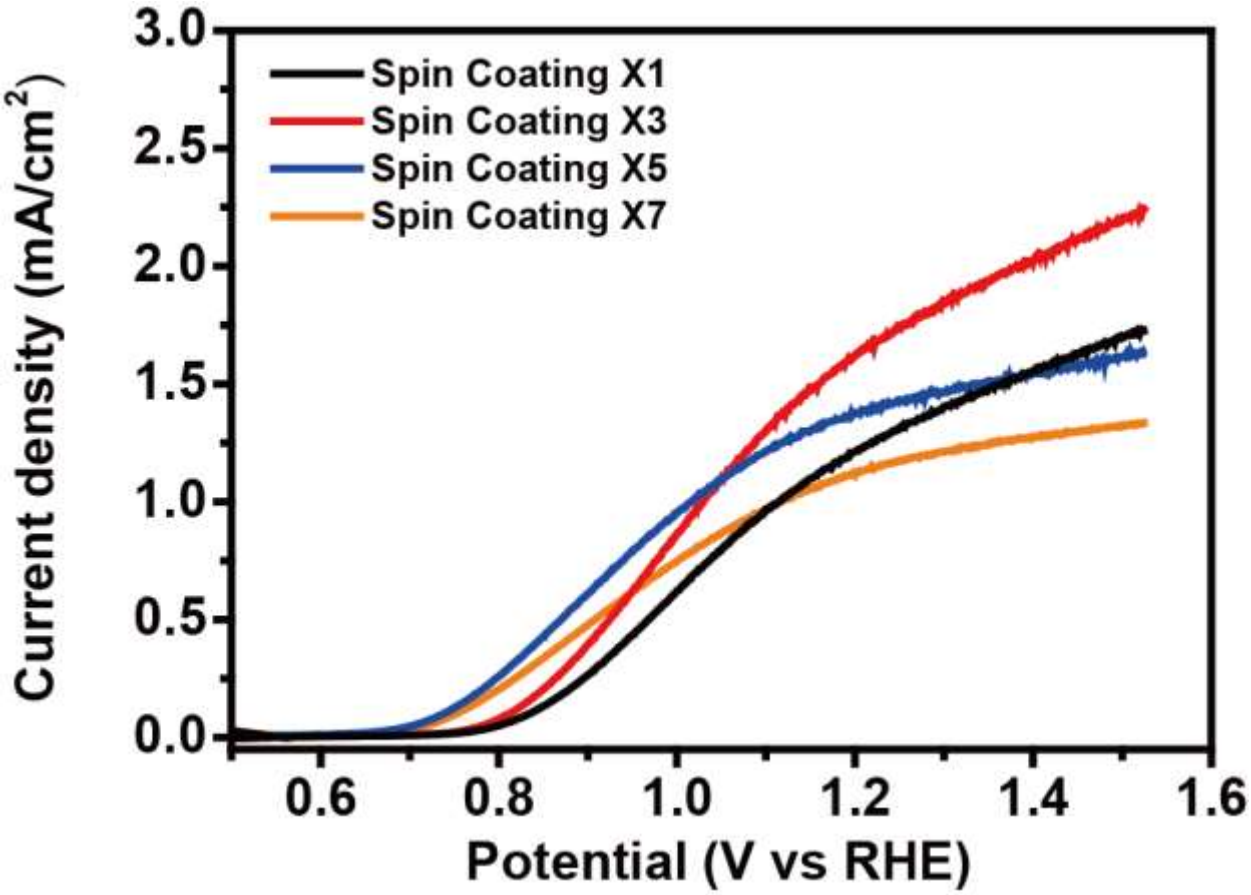

Figure S14. The curves for current density versus potential on N-doped NiAl nanosheets with different coating numbers.

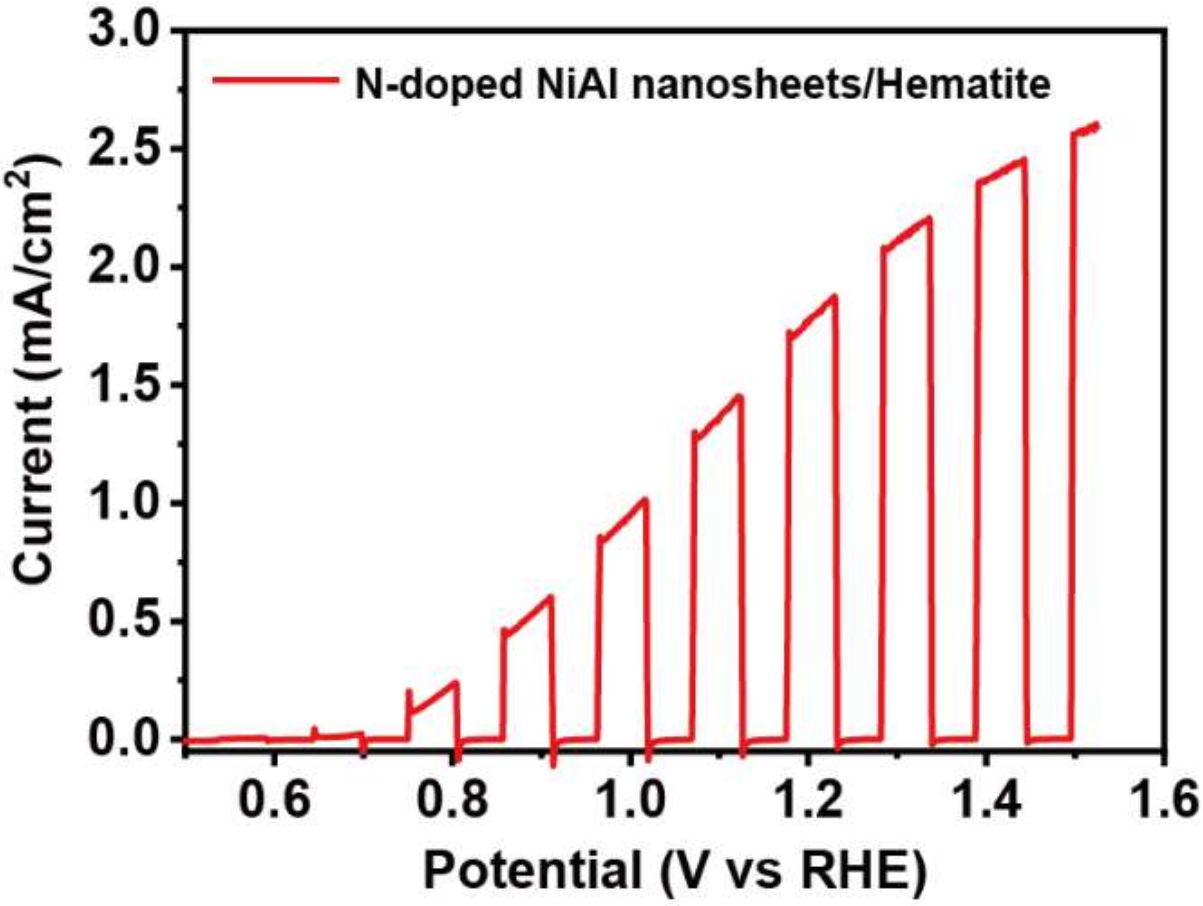

Figure S15. Chopped photocurrent-potential (I-V) curves for the PEC water oxidation for N-doped NiAl nanosheets/Hematite on FTO substrates.

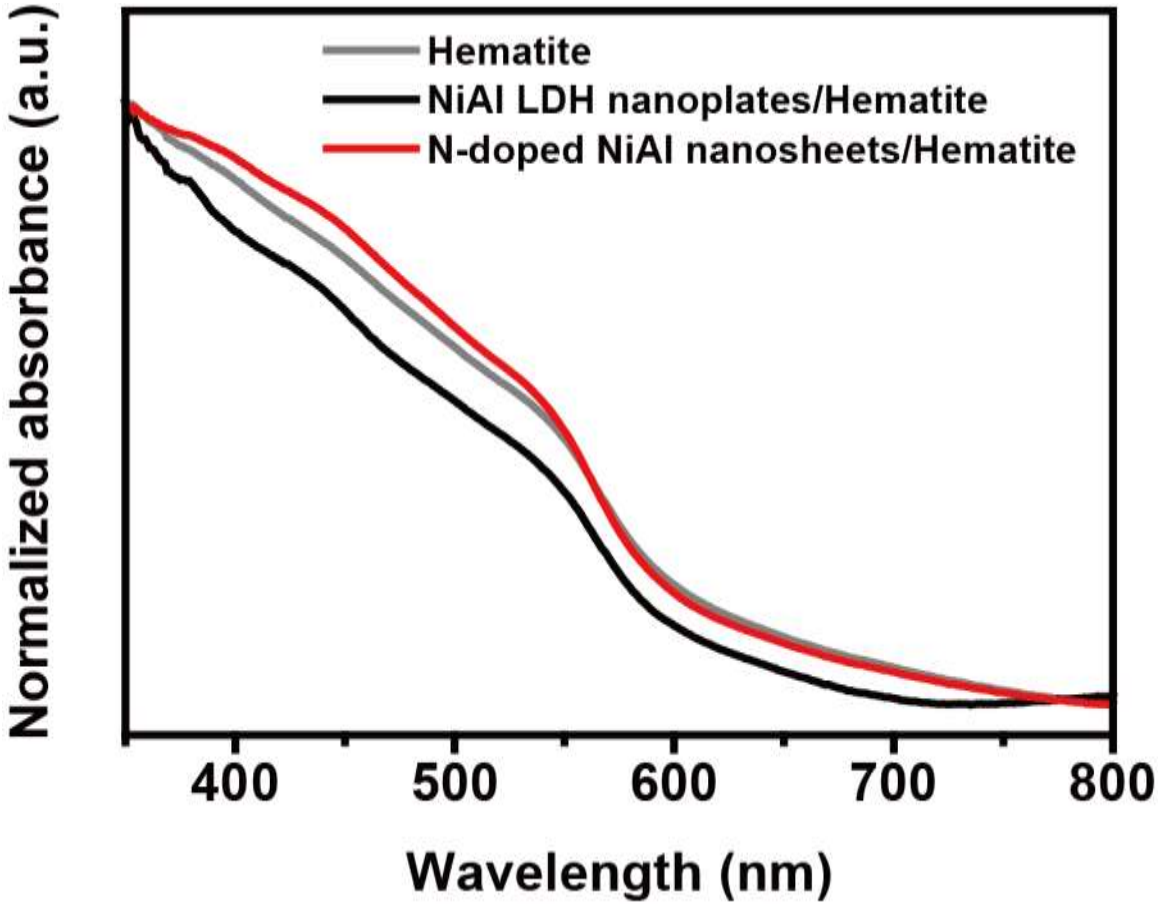

Figure S16. UV-Vis spectra of Hematite, NiAl LDH nanoplates/Hematite, and N doped NiAl nanosheets/Hematite photoanodes.

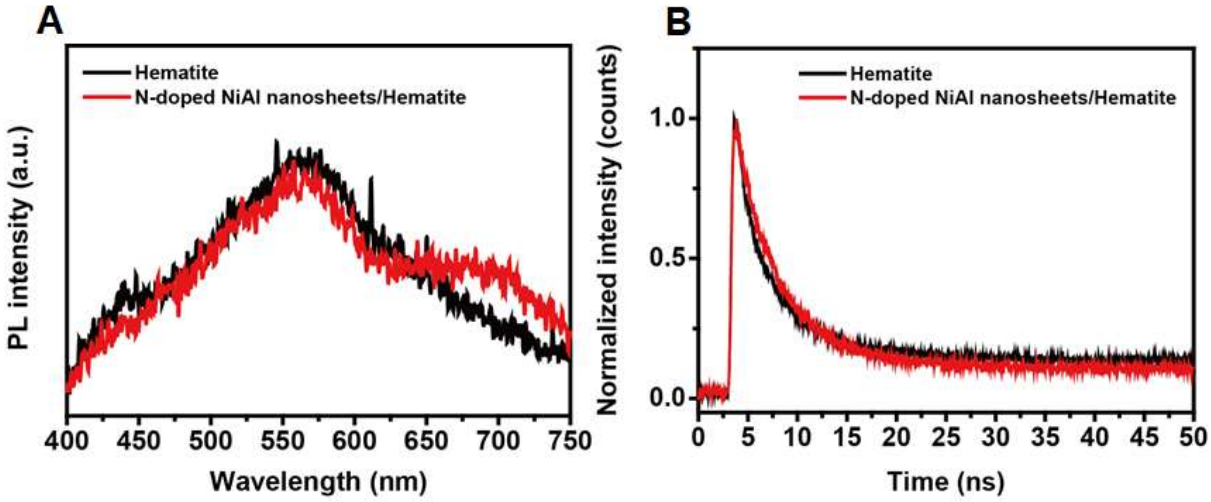

Figure S17. (A) PL intensity and (B) TCSPC of Hematite and N-doped NiAl nanosheets/Hematite photoanodes.

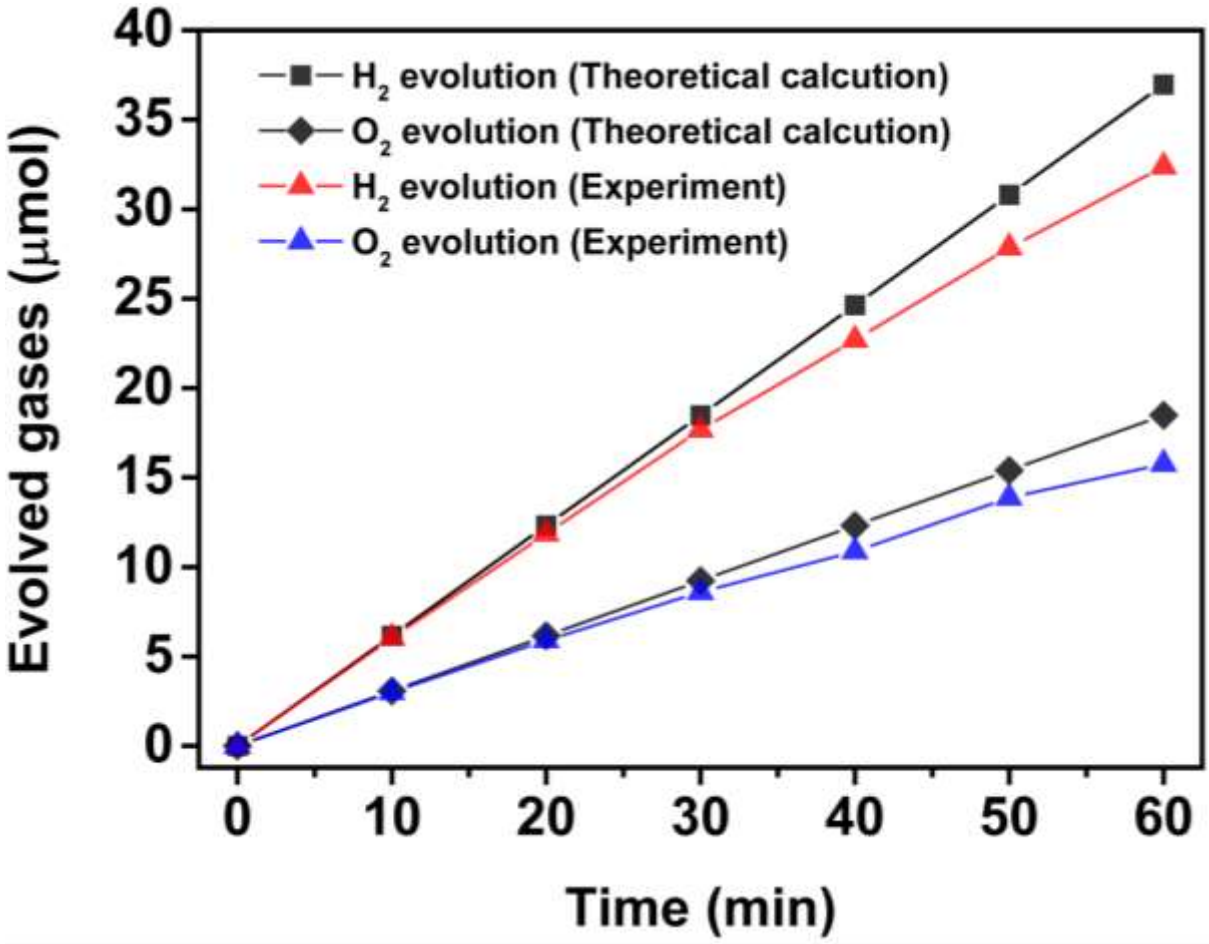

Figure S18. Gas evolution curves for N-doped NiAl nanosheets/Hematite under AM 1.5 G illumination at 1.23 V (vs RHE)

.

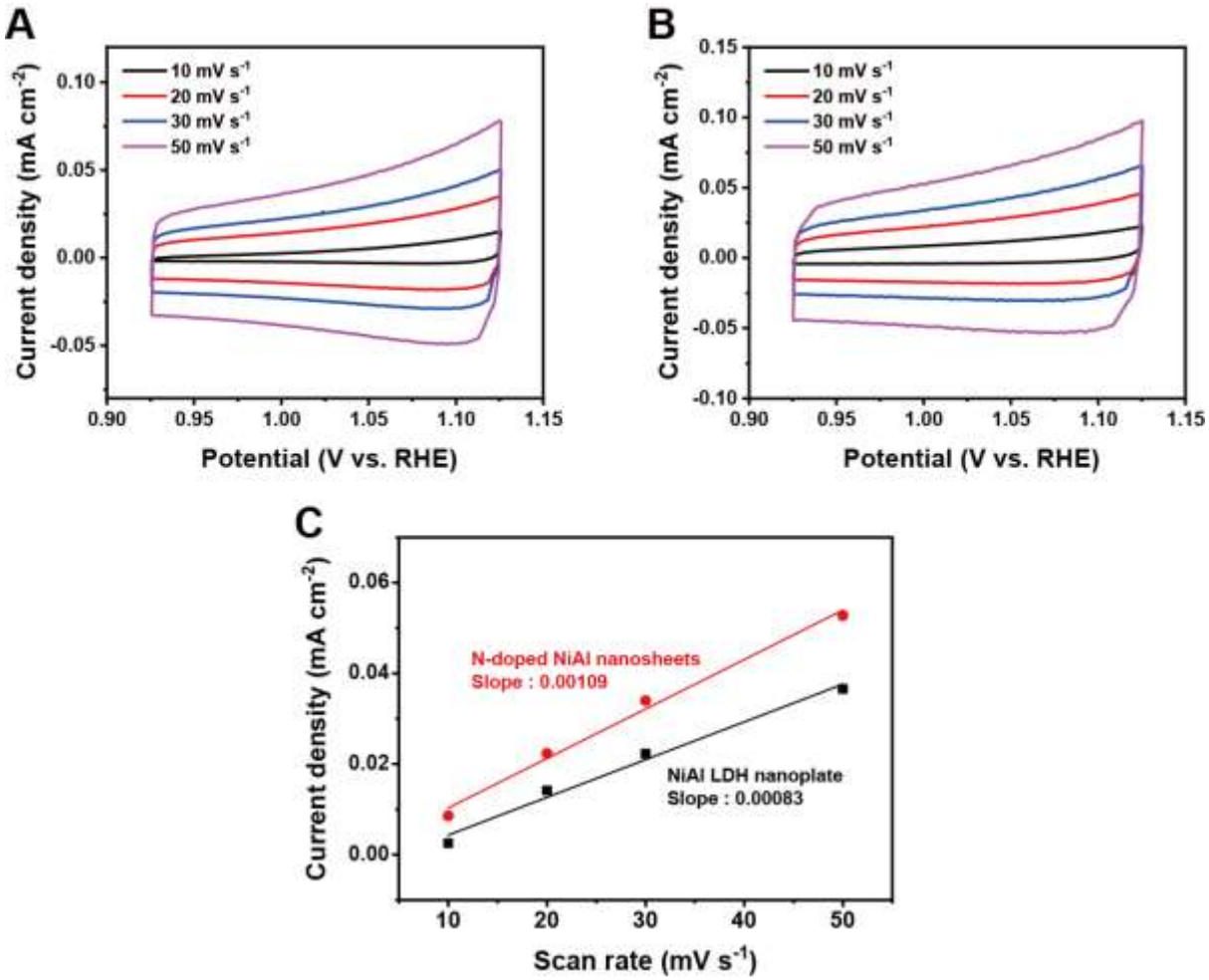

Figure S19. Electrochemical surface area (ECSA) tests of NiAl LDH nanoplate and N-doped NiAl nanosheets in 1M KOH condition. Cyclic voltammetry curves of (A) NiAl LDH nanoplate and (B) N-doped NiAl nanosheets with different scanning rates. (C) The capacitive current measured at 1 V vs. RHE was plotted as a function of scan rate.

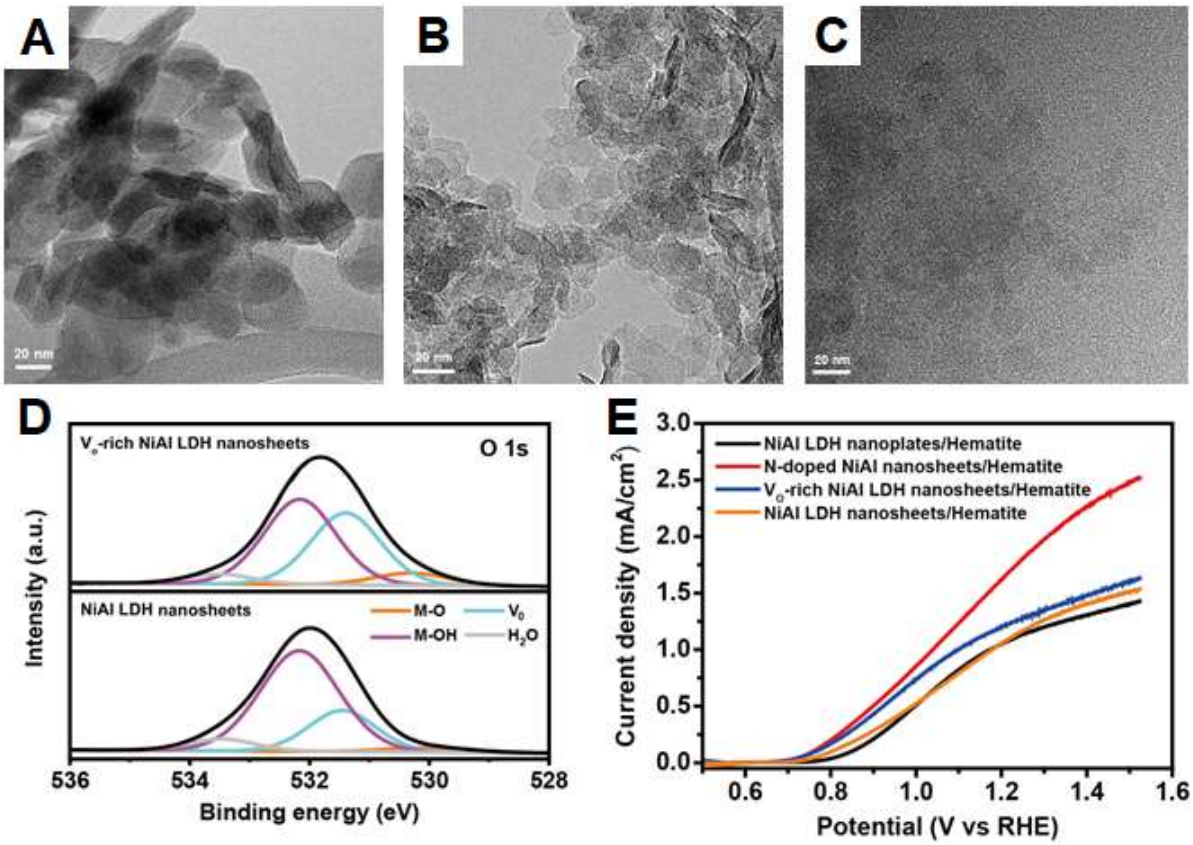

Figure S20. TEM images of (A) NiAl LDH nanoplates, (B) NiAl LDH nanosheets, and (C) oxygen vancancy-rich NiAl LDH nanosheets prepared through the chemical exfoliation. (D) The XPS spectra for O 1*s* orbitals of NiAl LDH nanosheets and oxygen vacancy-rich NiAl LDH nanosheets and (E) the linear sweep voltammetry curves compared with NiAl LDH nanoplates/hematite, NiAl LDH nanosheets/Hematite, oxygen vacancy-rich NiAl LDH nanosheets/Hematite, and N doped NiAl nanosheets/Hematite.

Section S3. Supporting Tables

Resistance	Samples	
	NiAl LDH nanoplates	N-doped NiAl nanosheets
R_1	17.42 Ω	25.75 Ω
R_2	182 Ω	161.6 Ω
R_3	257.4 Ω	60.8 Ω

Table S1. Fitted resistance results from Nyquist plots in Figure 4E.

Photoanode	Cocatalyst	Photocurrent (mA/cm^2)	Reference
Hematite	Au nanohole array	0.9	[1]
Hematite	Carbon nanodots+Co_3O_4	1.48	[2]
Hematite	Co-pi	0.93	[3]
Hematite	$Fe_{1-x}Ni_xOOH$	0.377(1% Sn-doped), 0.367 (1 % Zn-doped)	[4]
Hematite	FeOOH	1.21	[5]
Hematite	IrO_x	0.66	[6]
Hematite	$FeTiO_5$	0.78	[7]
Hematite	MnO_2	1.65 (P doping)	[8]
Hematite	$NiCeO_x$	0.68	[9]
Hematite	RGO+NiFe LDH	0.39	[10]
Hematite	$Ni(OH)_2$+IrO_2	1.75 (Ti doping)	[11]
Hematite	Cobalt catalysts	0.67 (Ti doping)	[12]
Hematite	FeOOH+Pt	2	[13]
Hematite	Zr underlayer+CTAB surfactant	0.8	[14]
Hematite	Ga_2O_3	0.42	[15]
Hematite	Co_3O_4	1.2	[16]
Hematite	$CO(OH)_2$+Co_3O_4	0.9	[17]
Hematite	Ni	1	[18]
Hematite	Ni-Bi	0.6	[19]
Hematite	$NiFeO_x$	0.58	[20]
Hematite	$Ni(OH)_2$	0.34	[21]
Hematite	TiO_2	0.65	[22]
Hematite	Zn acetate	1.1	[23]
Hematite	N-doped NiAl nanosheets	1.73	This work

Table S2. Comparison of photocurrents for various catalysts assembled with hematite.

Section S3. References

1 J. Li, S. K. Cushing, P. Zheng, F. Meng, D. Chu and N. Wu, *Nat. Commun.*, 2013, **4**, 1

2 P. Zhang, T. Wang, X. Chang, L. Zhang and J. Gong, *Angew. Chemie Int. Ed.*, 2016, **55**, 5851

3 M. Barroso, A. J. Cowan, S. R. Pendlebury, M. Grätzel, D. R. Klug and J. R. Durrant, *J. Am. Chem. Soc.*, 2011, **133**, 14868

4 A. Tsyganok, D. Klotz, K. D. Malviya, A. Rothschild and D. A. Grave, *ACS Catal.*, 2018, **8**, 2754

5 J. Y. Kim, D. H. Youn, K. Kang and J. S. Lee, *Angew. Chemie - Int. Ed.*, 2016, **55**, 10854

6 W. Li, S. W. Sheehan, D. He, Y. He, X. Yao, R. L. Grimm, G. W. Brudvig and D. Wang, *Angew. Chemie - Int. Ed.*, 2015, **54**, 11428

7 L. Wang, N. T. Nguyen and P. Schmuki, *ChemSusChem*, 2016, **9**, 2048

8 Q. Rui, L. Wang, Y. Zhang, C. Feng, B. Zhang, S. Fu, H. Guo, H. Hu and Y. Bi, *J. Mater. Chem. A*, 2018, **6**, 7021

9 H. Lim, J. Y. Kim, E. J. Evans, A. Rai, J. H. Kim, B. R. Wygant and C. B. Mullins, *ACS Appl. Mater. Interfaces*, 2017, **9**, 30654

10 F. Ning, M. Shao, S. Xu, Y. Fu, R. Zhang, M. Wei, D. G. Evans and X. Duan, *Energy Environ. Sci.*, 2016, 9

11 Z. Wang, G. Liu, C. Ding, Z. Chen, F. Zhang, J. Shi and C. Li, *J. Phys. Chem. C*, 2015, **119**, 19607

12 R. Franking, L. Li, M. A. Lukowski, F. Meng, Y. Tan, R. J. Hamers and S. Jin, *Energy Environ. Sci.*, 2013, **6**, 500

13 L. Wang, Y. Yang, Y. Zhang, Q. Rui, B. Zhang, Z. Shen and Y. Bi, *J. Mater. Chem. A*, 2017, **5**, 17056

14 P. S. Shinde, S. Y. Lee, S. H. Choi, H. H. Lee, J. Ryu and J. S. Jang, *Sci. Rep.*, 2016, **6**, 32436

15 T. Hisatomi, F. Le Formal, M. Cornuz, J. Brillet, N. Tétreault, K. Sivula and M. Grätzel, *Energy Environ. Sci.*, 2011, **4**, 2512

16 L. Xi, P. D. Tran, S. Y. Chiam, P. S. Bassi, W. F. Mak, H. K. Mulmudi, S. K. Batabyal, J. Barber, J. S. C. Loo and L. H. Wong, *J. Phys. Chem. C*, 2012, **116**, 13884

17 S. C. Riha, B. M. Klahr, E. C. Tyo, S. Seifert, S. Vajda, M. J. Pellin, T. W. Hamann and A. B. F. Martinson, *ACS Nano*, 2013, **7**, 2396

18 W. Cheng, J. He, Z. Sun, Y. Peng, T. Yao, Q. Liu, Y. Jiang, F. Hu, Z. Xie, B. He and S. Wei, *J. Phys. Chem. C*, 2012, **116**, 24060

19 Y. R. Hong, Z. Liu, S. F. B. S. A. Al-Bukhari, C. J. J. Lee, D. L. Yung, D. Chi and T. S. A. Hor, *Chem. Commun.*, 2011, **47**, 10653

20 C. Du, X. Yang, M. T. Mayer, H. Hoyt, J. Xie, G. McMahon, G. Bischoping and D. Wang, *Angew. Chemie - Int. Ed.*, 2013, **52**, 12692

21 K. M. H. Young and T. W. Hamann, *Chem. Commun.*, 2014, **50**, 8727

22 X. Yang, R. Liu, C. Du, P. Dai, Z. Zheng and D. Wang, *ACS Appl. Mater. Interfaces*, 2014, **6**, 12005

23 L. Xi, P. S. Bassi, S. Y. Chiam, W. F. Mak, P. D. Tran, J. Barber, J. S. Chye Loo and L. H. Wong, *Nanoscale*, 2012, **4**, 4430